







RESEARCH ARTICLE | MAY 10 2024

# Mechanically induced optical loss mechanism due to thermal expansion coefficient mismatch in micro-cavities with all-around stressor layers

Abdelrahman Z. Al-Attili ; Daniel Burt; Tasmia Rahman ; Zuo Li; Naoki Higashitarumizu ; Frederic Y. Gardes ; Yasuhiko Ishikawa ; Shinichi Saito 

 Check for updates

APL Photonics 9, 056104 (2024)

<https://doi.org/10.1063/5.0203305>

  
View  
Online

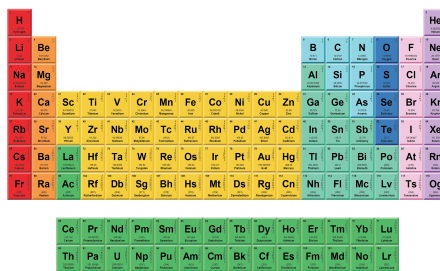
  
Export  
Citation

30 July 2024 12:54:23



THE MATERIALS SCIENCE MANUFACTURER®

**Now Invent.™**



American Elements  
Opens a World of Possibilities

...Now Invent!

[www.americanelements.com](http://www.americanelements.com)

© 2024 American Elements is a U.S. Registered Trademark

# Mechanically induced optical loss mechanism due to thermal expansion coefficient mismatch in micro-cavities with all-around stressor layers

Cite as: APL Photon. 9, 056104 (2024); doi: 10.1063/5.0203305

Submitted: 12 February 2024 • Accepted: 25 April 2024 •

Published Online: 10 May 2024



View Online



Export Citation



CrossMark

Abdelrahman Z. Al-Attili,<sup>1,2,a)</sup> Daniel Burt,<sup>1</sup> Tasmia Rahman,<sup>1</sup> Zuo Li,<sup>1</sup> Naoki Higashitarumizu,<sup>3</sup> Frederic Y. Gardes,<sup>1</sup> Yasuhiko Ishikawa,<sup>4</sup> and Shinichi Saito<sup>1</sup>

## AFFILIATIONS

<sup>1</sup>Sustainable Electronic Technologies, Department of Electronics and Computer Science, University of Southampton, Southampton SO17 1BJ, United Kingdom

<sup>2</sup>Department of Energy Engineering, School of Engineering Technology, Al Hussein Technical University, Amman 11831, Jordan

<sup>3</sup>Department of Materials Engineering, University of Tokyo, 7-3-1 Hongo, Bunkyo-Ku, Tokyo 113-8656, Japan

<sup>4</sup>Department of Electrical and Electronic Information Engineering, Toyohashi University of Technology, 1-1 Hibarigaoka, Tempaku, Toyohashi 441-8580, Japan

<sup>a)</sup> Author to whom correspondence should be addressed: [AbdAttili@HTU.edu.jo](mailto:AbdAttili@HTU.edu.jo)

## ABSTRACT

Various excitation-induced loss mechanisms have been identified during the development of direct-gap semiconductor lasers. Recently, indirect-gap laser sources, particularly germanium (Ge) or GeSn based, have emerged due to silicon industry compatibility. Tensile strain is crucial for optical gain or low-threshold room-temperature operation in such media. This study investigates an excitation-induced optical loss mechanism of mechanical origin in Ge-based micro-cavities with all-around stressor layers, a popular platform for strain-engineered laser sources. Using Raman spectroscopy, photoluminescence, and simulations, we find that excitation lowers the optical gain by altering the strain profile. Heating causes Ge micro-cavities to expand within a constraining stressor layer, inducing compressive strain, which is explained by the mismatch in thermal expansion coefficients.

© 2024 Author(s). All article content, except where otherwise noted, is licensed under a Creative Commons Attribution (CC BY) license (<https://creativecommons.org/licenses/by/4.0/>). <https://doi.org/10.1063/5.0203305>

## I. INTRODUCTION

Germanium (Ge) and GeSn alloys have been the focus of researchers in the search for a potential optical gain medium compatible with the current complementary metal-oxide-semiconductor (CMOS) industry.<sup>1-5</sup> Although this research pathway was established to investigate Ge platforms,<sup>6-23</sup> the current efforts are concentrating on GeSn alloys.<sup>3,24-27</sup> In both trends, the aim is to provide direct-gap Ge-based material.<sup>24,28,29</sup> To realize this in pure Ge, the application of tensile strain has been widely investigated, overshadowing other possible techniques such as *n*-type doping.<sup>30,31</sup> *n*-type doping was initially proposed to fill the indirect-gap (L) valley with electrons, reducing the injection requirements to reach transparency.<sup>4-6,32,33</sup> Yet, achieving high doping concentration levels without degrading the Ge crystalline quality is not

straightforward,<sup>34,35</sup> and the understanding of doping effects on electrical and optical losses is not fully developed yet.<sup>36</sup> Tensile strain, on the other hand, has provided consistent results throughout the research community, confirming optical gain and lasing.<sup>24-27,37,38</sup>

Novel fabrication techniques imposing tensile strain onto Ge structures were developed,<sup>12,15,19,39</sup> compromising multiple important design factors such as the necessity of high tensile-strain values, the nature of this strain being uniaxial or biaxial, providing optical confinement, and the suitability for electrical pumping. Ge can be transformed into a direct-gap material using ~4.5% and 1.7% uniaxial<sup>38,40,41</sup> and biaxial<sup>42,43</sup> tensile strain values, respectively. Efficient room-temperature (RT) lasing of Ge requires even higher strain values, resulting in an energy difference of 150 meV between the direct (Γ) and indirect (L) valleys of the conduction band.<sup>24</sup>

Practical devices relied mainly on two techniques for this purpose: releasing pre-stressed Ge films with engineered dimensions<sup>41,44</sup> and depositing stressor layers, or stress liners, according to the CMOS fabrication terminology.<sup>3,15,16,24–26</sup> Freestanding Ge structures with tapered pads, also known as the geometrical amplification technique, relying on large Ge pads pulling a middle Ge section with smaller dimensions, have been proposed for achieving such high strain values.<sup>41</sup> Although strain values up to 5.7% have been reported using this technique,<sup>41</sup> this uniaxial value is comparable to a biaxial strain value of ~2% achieved using stressor layer techniques.<sup>28,42,45</sup> The advantages of the freestanding Ge films, though, include their suitability for electrical pumping and better heat dissipation through the pads that may be in direct contact with the bulk Si wafer.<sup>46</sup> Heat dissipation is crucial for lasing; in fact, recently, it has been the main factor being investigated in reducing the threshold in GeSn micro-cavities, as will be discussed below.<sup>3,24–27</sup> The dissipation of heat through a freestanding Ge film connected to larger pads on both sides is expected to be easier than the stressor layer technique. The latter relies on the deposition of a pre-stressed film such as SiN or SiO<sub>2</sub> around the Ge-based cavity. Given that the thermal conductivity of such stressor layers is lower than that of Ge, in addition to being surrounded by air, the heat dissipation path is worsened in-plane of the cavity. In fact, the best heat sinking path would be through the substrate below the Ge structure.<sup>3,24–27</sup> Stressor layers have been used on Ge-based waveguides<sup>47</sup> and micro-cavities,<sup>15,17</sup> resulting in biaxial strain. An all-around stressor layer technique was proposed to improve the uniformity of tensile strain along the three spatial directions<sup>18</sup> and has been popular since then, especially with micro-cavities, providing simple structures with good optical confinement capabilities. Although high biaxial tensile strain values up to ~2% were achieved using such structures,<sup>42,45</sup> resulting in optical modes with good quality factors, efficient RT lasing has not been demonstrated in pure Ge yet. It was obvious then that imposing further tensile strain is not feasible as the complexity of achieving a slight increase in strain values is immense, and the corresponding reduction in the lasing threshold would still be considered humble.

Hence, the shift toward investigating GeSn alloys, given that a direct bandgap can be achieved by tuning the Sn content percentage.<sup>25,27</sup> Consistent lasing at cryogenic temperatures was subsequently reported in GeSn cavities.<sup>3,24–27</sup> Research efforts have been focused since then on reducing the lasing threshold in order to achieve efficient RT operation. The tensile strain has emerged once again as a possible solution<sup>24</sup> due to the strain-induced deformation of the band edges toward creating a direct-gap GeSn alloy, similar in principle to Ge. However, this time a combination of Sn content tuning and tensile strain has been utilized in order to create an effective light-emitting direct-gap medium.<sup>24–26</sup> This reduces the requirements of the Sn percentage, enhancing the crystalline quality that is decreased with the Sn to Ge ratio, as the tensile strain is used to compensate for the remaining Sn content required to achieve the direct-gap characteristic.<sup>24</sup> It also meant that a reasonable tensile strain value was required. For instance, a combination of 5.4% Sn content in a GeSn micro-cavity with 1.4% tensile strain applied using an all-around stressor layer resulted in a promising low lasing threshold.<sup>24</sup>

Efficient RT lasing of GeSn micro-cavities has another challenge to overcome, namely, heating effects. RT lasing of

direct-gap GeSn micro-cavities is not straightforward because pumping requirements to reach transparency increase with operating temperature as the losses to be compensated for increase while pumping itself heats up the device even more. This indicates that achieving reliable RT lasing at the current gain levels requires mitigating the heating effects with better heat sinking techniques.<sup>24,27</sup> As most of the recent lasing reports of GeSn micro-cavities relied on an all-around low-thermal-conductivity stressor layer,<sup>3,24–27</sup> the most suitable heat-sinking path is obviously through the pedestal to the substrate. Several works have exploited metallic pedestals to hold the GeSn micro-cavities instead of standard wafer materials.<sup>24–26</sup> A recent study has demonstrated reducing the RT lasing threshold in non-strained GeSn micro-cavities through a systematic heat-management comparison.<sup>27</sup> The technique relied on using lower-Sn layers around a high-Sn gain medium in a heterostructure for better thermal dissipation, in addition to using an AlN pedestal, which resulted in a lower lasing threshold compared to the same structure on a Ge pedestal, explained by the higher thermal conductivity of AlN compared to Ge.<sup>27</sup> Although the current trend suggests designing structures to bear with the high temperatures resulting from extreme pumping by dissipating the heat into the substrate, it is well understood that heating effects mainly impact carriers and optical losses, affecting the threshold value itself. Previous studies on Ge micro-disks have pointed out heating effects as a major obstacle preventing lasing; for example, the redshift in the absorption band-edge and free-carrier absorption losses may cause a drastic drop in the quality factors of confined modes.<sup>10</sup>

In this work, we investigate a new type of optical loss of mechanical origin: the effect of the heat generated due to excitation on the tensile-strain profile within Ge-based micro-cavities with an all-around stressor layer. Such an interaction is relevant to Ge-based light-sources as the strain corresponds directly to the optical gain value, if not the main source of the optical gain. Ge micro-gear cavities with all-around stressor layers on silicon (Si) pedestals are used as exemplar structures, similar in principle to the recently popular configurations of GeSn micro-cavities with successful lasing reports. Consequent finite-element method (FEM) simulations combining the effects of strain and heating were conducted to investigate the mechanical behavior of the cavities undergoing optical excitation. The simulations show that the strain profile within the cavities is remarkably altered due to pumping, resulting in a more compressive strain distribution. This heat-induced strain variation is then reflected onto photoluminescence (PL) and Raman data. Whispering-gallery modes (WGMs) with different radial orders and, therefore, a different spatial distribution of the electric fields were found to experience different degradation behavior with pumping. This is due to the variation in the overlap between the altered strain profiles upon heating and the optical modes. We believe that this investigation sets up an important consideration for the design of light sources with strain-originated optical gain.

## II. THE PLATFORM: MICRO-CAVITIES WITH ALL-AROUND STRESSOR LAYERS

Ge micro-gear cavities with all-around SiO<sub>2</sub> stressor layers on Si pedestals serve as exemplar structures. Ge micro-gears with periods ( $m$ ) ranging from 14 to 21 were fabricated, with a period defined

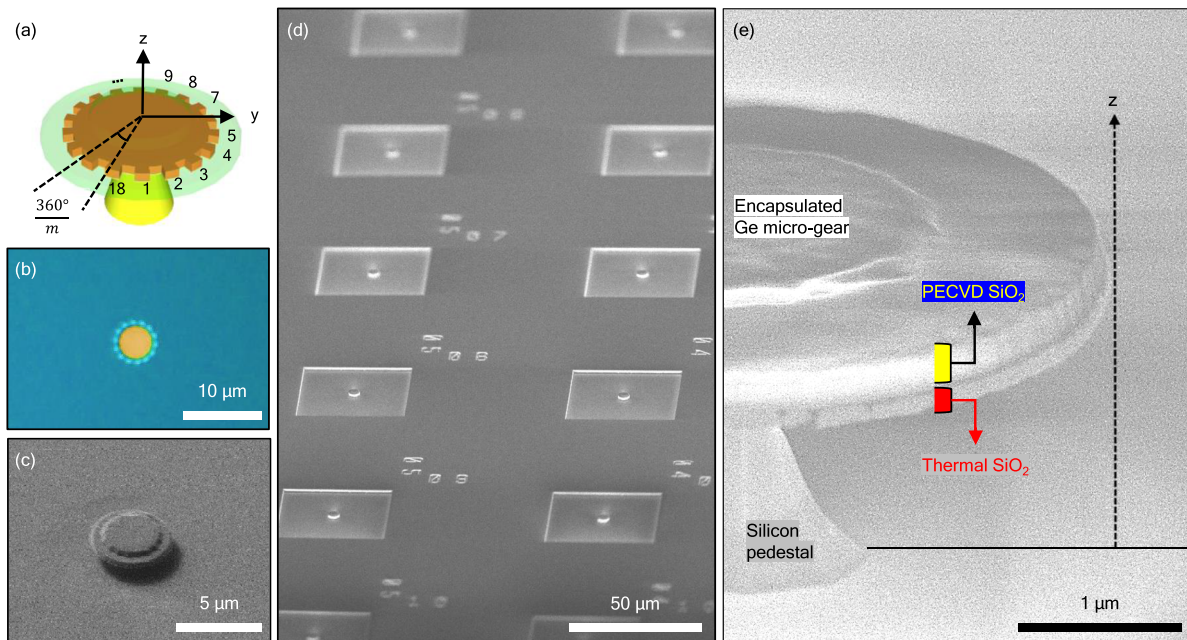


**FIG. 1.** Ge micro-cavities with all-around stressor layers. (a) 3D sketch defining micro-gear periods. (b) Optical and (c) scanning-electron microscopy images. (d) Side-view of the bulk-Si cylindrical pillars holding the micro-cavities before etching them into pyramidal pedestals. (e) Upward deformation of the final device upon the formation of the pyramidal pedestal due to the higher initial stress of the thermal  $\text{SiO}_2$  layer.

as shown in Fig. 1(a). The stack consists of 145-nm plasma-enhanced chemical-vapor deposition (PECVD)  $\text{SiO}_2$  on top of 200-nm Ge on 20-nm Si. The bottom dioxide layer is thermally grown during the Ge on Si-on-insulator (SOI) wafer production, with a thickness of 145 nm matching that of the top PECVD oxide. The diameter of the Ge micro-gears is  $4 \mu\text{m}$ , while the diameter of the  $\text{SiO}_2$  encapsulation extends by 600 nm. The cavity encapsulated with the all-around stressor layer sits on a Si pedestal with a 500-nm wide top. Details on the fabrication process can be found elsewhere.<sup>13,14</sup> Figures 1(b) and 1(c) show an optical image of a Ge micro-gear from the top and a 3D view of the final structure using scanning-electron microscopy (SEM). A critical drawback of this structure, compared to the commonly used structures for GeSn-based micro-cavities,<sup>3,24–27</sup> is that the cavity region is isolated from the pedestal by the dioxide layer, degrading the thermal dissipation path into the substrate. This is shown in Figs. 1(d) and 1(e), where inductively coupled plasma (ICP) etching is used to define the Si pillars [Fig. 1(d)], with the dioxide layer holding the cavity on top, then anisotropic wet-etching is performed to under-etch the dioxide, forming Si pedestals as shown in Fig. 1(e). A Si pillar [Fig. 1(d)] with a diameter equal to the cavity's diameter would provide better thermal dissipation, yet optical confinement of the WGMs would be challenging, thus releasing the cavity's circumference is required [Fig. 1(e)]. This release of the pre-stressed  $\text{SiO}_2$  encapsulation causes it to expand, imposing tensile strain on the embedded Ge micro-cavity. Interestingly, the final structure deforms upward due to the higher initial stress of the thermal dioxide compared to the PECVD layer. This deformation affects the strain distribution, hence the optical gain, within the Ge region, as will be discussed later.

### III. SPECTRA OF EVEN AND ODD-PARITY MICRO-GEARS

Resonant modes of Ge micro-gears with physical periods ranging from 14 to 21 were observed using PL measurements, as shown in Fig. 2. The main PL peak in all devices corresponds to the direct Ge bandgap with a slight biaxial strain of around 0.3%, as confirmed by simulations. Sharp-peak resonances were identified as WGMs with different azimuthal and radial orders. WGM orders are assigned in Fig. 2 using a two-number notation: the first number corresponds to the azimuthal order, which is the number of full wavelengths of the WGM, and the second number corresponds to the radial order, which is the number of field maxima along the radius of the micro-gear. Modes with higher radial orders have a considerable portion of the electric field squeezed into the inner regions of the micro-gear, while the first radial order modes have the main portion of the electric field at the circumference of the cavity. Micro-gears with 17 and 18 physical periods confined modes with the highest quality factors.<sup>48,49</sup> The micro-gear with 17 physical periods resulted in the best quality factor of  $\sim 715$  at a wavelength of 1790 nm and a pump power of 2 mW. Odd-parity gears seem to filter out the WGMs with the first radial order in the observed wavelength region. For instance, the WGMs within the 17-period gear are identified as (16,2), (12,3), and (11,3) occurring at 1665, 1724, and 1790 nm, respectively. Meanwhile, the WGMs in the 18-period gear, an even-parity gear, are (20,1), (19,1), and (18,1) occurring at 1670, 1728, and 1793 nm, respectively. This difference in the radial order affects the spatial overlap between the electric field and the tensile-strain profile in the micro-gear, influencing the optical gain seen by the modes. Moreover, WGMs will experience different

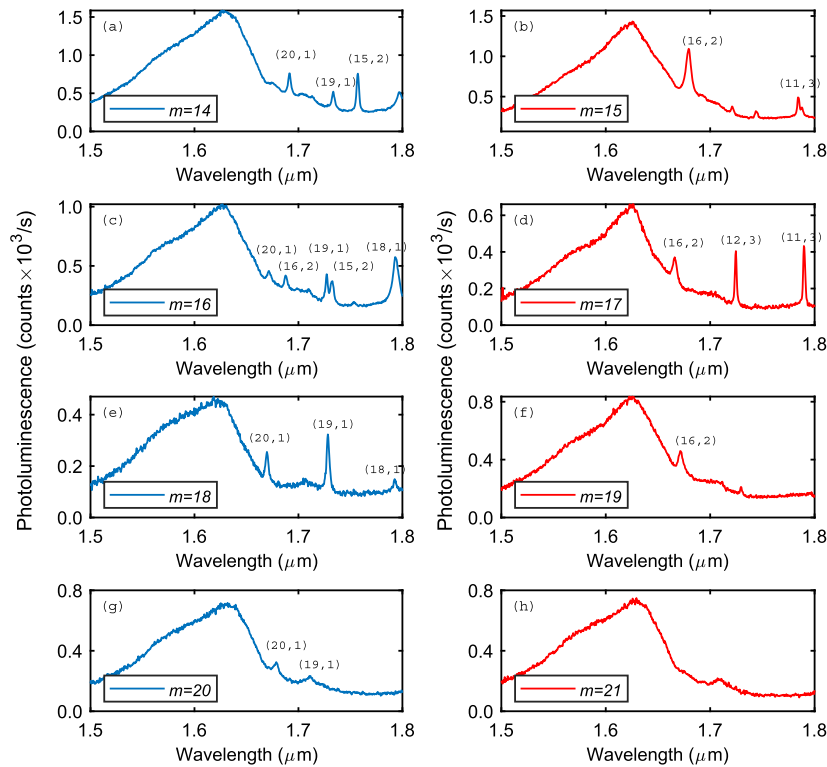


FIG. 2. PL spectra of micro-gear cavities with different periods. WGMs of higher radial orders are confined in odd-parity micro-gears.

scattering losses as the first-radial-order modes will interact with the etched gear surface and lower-strain regions at the circumference. On the other hand, higher-radial-order WGMs are in closer proximity to the excitation region, assuming pumping is centered in the middle of the cavity.

#### IV. EXCITATION-INDUCED STRAIN VARIATION

##### A. Finite-element method simulations

Three-dimensional FEM simulations were conducted in two consequent stages: first, the initial strain distribution in the devices after fabrication due to the release of the compressively stressed  $\text{SiO}_2$  layers was simulated. Ge micro-gears of  $2 \mu\text{m}$  radius and 50-nm-deep etched gear teeth were modeled, where the gear teeth depth is the difference between the inner and outer radius values of the gear, encapsulated with an all-around  $\text{SiO}_2$  layer of  $2.3 \mu\text{m}$  radius. This all-around stressor layer consisted of a 145-nm-thick  $\text{SiO}_2$  layer below (above) the Ge cavity with an initial compressive stress of 1000 MPa (500 MPa), representing thermally grown (PECVD) layers. The Ge layer has an initial tensile strain value of 0.2%.<sup>50</sup> The device boundaries were set as free boundaries, except for the bottom of the Si pedestal holding the cavity. The resulting steady-state distribution of the strain values due to the initial stresses represents the devices before excitation, as shown in Fig. 3(a). The sketch is deformed to visualize the initial state of the device, and a cross-sectional plane is highlighted in the

middle of the micro-gear to illustrate the strain variation across the thickness of the cavity. The cavity is deformed upward, similar to the SEM image shown in Fig. 1(e), due to the higher compressive stress in the thermal  $\text{SiO}_2$  below the Ge layer compared to the PECVD oxide on the top. The initial stress value was estimated to be 1000 MPa (500 MPa) in the thermal (PECVD)  $\text{SiO}_2$ , respectively, using wafer-curvature measurements and Stoney's formula.<sup>51</sup> This variation results in higher tensile strain values at the bottom side of the cavity, as evident in Fig. 3(a), with volumetric strain values approaching 0.8% compared to 0.4% within the top regions.

Second, the result from the previous stress-strain simulation was used as an initial condition for the next stage, where the effect of heating (excitation) is modeled. Excitation is modeled as a  $2\text{-}\mu\text{m}$ -diameter spot on the top surface of the device (a uniform beam profile was assumed), representing a boundary heat source of 2 mW power. The initial temperature condition of the device was set to RT. The boundary conditions constrained the temperature at the bottom of the Si pedestal to RT, representing the heat-sinking path. The thermal expansion coefficients used for Ge, Si, and  $\text{SiO}_2$  were  $5.9 \times 10^{-6}$ ,  $2.6 \times 10^{-6}$ , and  $0.5 \times 10^{-6} \text{ K}^{-1}$ , respectively.<sup>52–55</sup> A transient study of the heating effects on the strain profile was conducted to visualize the dynamic behavior of the cavity. Figure 3(b) presents the same structure upon excitation with a 2 mW laser beam of a  $2 \mu\text{m}$  diameter from the top after reaching a steady state condition. The heat-induced strain variation is evident as the structure

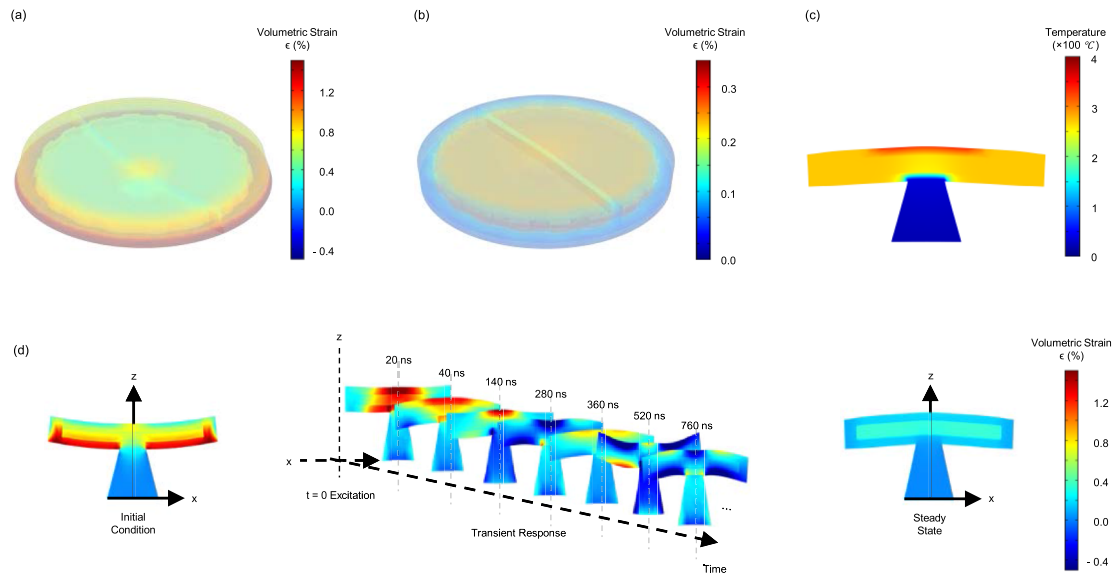


**FIG. 3.** Simulated strain profile: (a) before and (b) after excitation. (c) Temperature cross-sectional distribution based on 2 mW excitation. (d) Transient response of the cross-sectional strain profile. The cavity undergoes several deformations as the inner and outer materials have dissimilar thermal expansion coefficients until a steady-state condition is reached.

is deformed downward, with two main outcomes to highlight: first, the strain within the Ge layer is reduced to  $\sim 0.35\%$ , and second, the strain is mostly uniform across the cavity. These two effects arise from the fact that Ge expands at a higher rate ( $\sim 12\times$ ) compared to the encapsulating stressor layer due to the higher thermal expansion coefficient. This constrains the expansion of the heated Ge cavity, imposing compressive forces that reduce the tensile strain values. The uniformity of the new strain distribution supports this hypothesis, as the new deformation is mainly governed by the thermal expansion. Downward deformation after excitation is probably due to the top layers being at higher temperatures compared to the bottom ones. In this context, it is important to mention that the thermal expansion coefficients of the thermal and PECVD  $\text{SiO}_2$  layers are assumed to be equal for simplicity. In reality, the thermal expansion coefficient of the PECVD  $\text{SiO}_2$  varies depending on the deposition process parameters and is often reported to range from nearly 1 to 5 times that of the thermal  $\text{SiO}_2$ .<sup>53–55</sup> If the highest reported value is used for the top PECVD  $\text{SiO}_2$  in our structure ( $\sim 2.6 \times 10^{-6} \text{ K}^{-1}$ ),<sup>54,55</sup> then the upper part of the structure is expected to expand more than the lower part, as the lower thermal  $\text{SiO}_2$  expands at a rate of  $0.5 \times 10^{-6} \text{ K}^{-1}$ .<sup>53</sup> This causes the cavity to undergo a slightly increased downward deformation compared to Fig. 3(b). To quantify this effect, it can be summarized that if the expansion coefficients are assumed to be equal, which is the case in Fig. 3(b), then the strain values upon excitation measured at the top, middle, and bottom of the Ge cavity layer (at a radius of  $1.5 \mu\text{m}$ ) are found to be 0.355%, 0.352%, and 0.35%, respectively. On the other hand, if the PECVD layer expansion coefficient is assumed to be five times larger than that of the thermal layer ( $\sim 2.6 \times 10^{-6} \text{ K}^{-1}$ ),<sup>54,55</sup> then the strain values upon excitation measured at the top, middle, and bottom of the Ge cavity layer (at a radius of  $1.5 \mu\text{m}$ ) are found to be 0.39%, 0.3725%, and 0.36%, respectively. The differences between

both cases are not significant— $\sim 0.035\%$  and  $0.01\%$  at the top and bottom layers, respectively. This is expected as the cavity's expansion is restricted by the slow-expanding bottom thermal oxide layer. Yet, the values also clearly indicate additional downward deformation if the higher thermal expansion coefficient value is used for the PECVD layer, as the tensile strain value at the top and the non-uniformity of the strain values across the Ge thickness are both higher.

Figure 3(c) plots the sectional distribution of temperature due to excitation, indicating that the cavity heats up to  $\sim 300^\circ\text{C}$  when excited with a 2 mW laser beam. The laser beam is assumed to be concentric to the cavity; hence, the temperature is highest in the middle-top regions. Heat is mainly dissipated through the pedestal, as the Si path has less thermal resistance compared to  $\text{SiO}_2$  and air. In addition to the heating effects on conventional optical and carrier losses, such as free-carrier absorption and the redshift of the absorption band-edge,<sup>10</sup> the strain-induced optical gain is degraded. WGMs with different radial orders along the radius of the cavities will undergo a different change in the overlap between the electric field and the new strain values. Moreover, the temperature seen by each mode will vary depending on the vicinity of the electric field to the central regions, assuming the excitation is performed in the middle. It is worth mentioning that this transition is not a zero-order response in terms of time. Figure 3(d) plots this transient process as seen in cross-sectional views. A cross-section at time  $t = 0$ , representing the initial state before excitation, is shown on the left, followed by consequent sections captured at different time steps, while the steady state result is shown on the right with a downward deformed structure. During this transient process, the structure undergoes mechanical oscillations, causing the micro-cavity to deform in different directions, alternating the strain profile in nano-second time frames. This transient response is a higher-order response in

terms of time dependence, as the initial conditions are not strain-free, resulting in a spring-like effect that dampens the transition. Simulations indicate that the steady state condition is reached after  $\sim 5 \mu\text{s}$  in this particular case. Such fast behavior is not observable in conventional Raman or PL measurements.

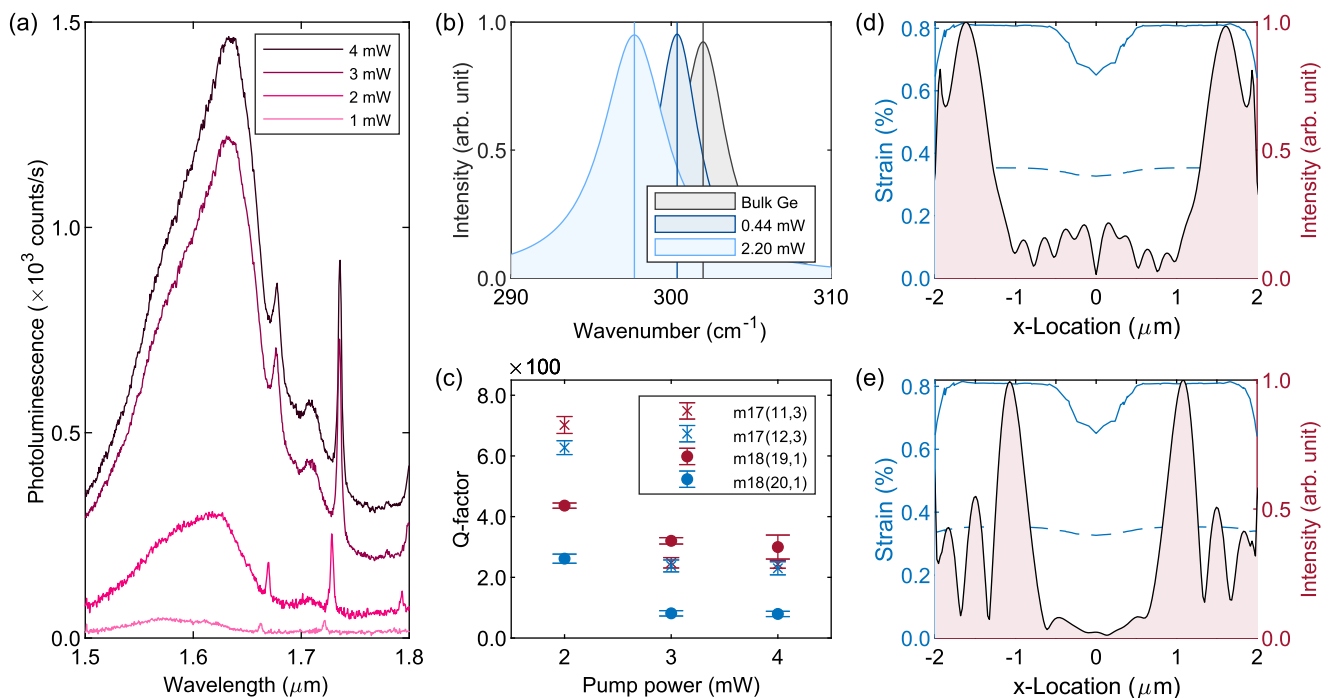
## B. Photoluminescence

Figure 4(a) plots the emission spectra of an 18-period micro-gear under different excitation power values (785 nm wavelength). An 18-period gear is chosen as an example as the azimuthal orders of the WGMs within the Ge direct-gap are around the physical-period order of the gear, resulting in better quality factors.<sup>48,49</sup> Transverse electric (TE) modes, namely,  $\text{TE}_{(18,1)}$ ,  $\text{TE}_{(19,1)}$ , and  $\text{TE}_{(20,1)}$ , are observable in the spectra, with  $\text{TE}_{(19,1)}$  having the best quality factor. Increasing the excitation power from 1 to 4 mW increases the PL emission intensity. The main peak corresponds to  $\Gamma$ -heavyhole emissions.<sup>28</sup> A redshift in the emission peak is expected with the excitation due to heating.<sup>56</sup> For instance, the average temperature of the micro-gear is simulated to be 271.5, 397.1, and 522.8 °C at 2, 3, and 4 mW excitation power values, respectively. Taking the 2 mW case as a reference, with the  $\Gamma$ -heavyhole peak at 1626 nm, the corresponding redshifted peaks at 3 and 4 mW excitation can be calculated at 1687.1 and 1753.1 nm, respectively, assuming the temperature sensitivity coefficient to be  $-2.2 \times 10^{-4}$  eV/K for Ge on Si films.<sup>56</sup> The measured spectra, however, have the corresponding peaks at 1633 and 1635 nm, respectively, as evident in

Fig. 4(a). The measured redshift values of 7 nm (3 mW) and 9 nm (4 mW) are remarkably less than the theoretical estimations of 61 nm (3 mW) and 127 nm (4 mW). This difference can be explained by the contradicting effects of heating (redshift) and the reduction of tensile strain (blueshift), as predicted by simulations. Hence, the PL peak behavior will depend on the net effect of temperature and strain, which will be analyzed according to the Raman spectra in Fig. 4(b). For this device, the quality factor of  $\text{TE}_{(19,1)}$  was higher than  $\text{TE}_{(20,1)}$ , probably due to the modes' wavelengths relative to the  $\Gamma$ -lighthole emission peak.<sup>10</sup> The quality factors of both WGMs degraded with excitation and reached a nearly fixed value above 3 mW excitation, as shown in Fig. 4(c). It is to be noted that the refractive index of Ge is also temperature dependent. However, an increase in the Ge refractive index is expected as the temperature increases, which does not explain the decrease in the quality factor.<sup>57,58</sup>

## C. Raman spectroscopy

Figure 4(b) plots the Raman spectra of the same device excited with 0.44 and 2.2 mW laser power (532 nm wavelength), with the bulk Ge spectrum included as a reference. Increasing the excitation power results in an increased Raman shift toward lower wavenumbers, or higher wavelengths, and a proportional broadening of the Raman curve.<sup>10,12</sup> The strain values can be deduced from the Raman shift using proportionality factors that are reported in the literature.



**FIG. 4.** Correlation of optical characteristics and strain variation upon excitation. (a) PL and (b) Raman spectra of an 18-period micro-gear using different excitation powers. (c) Quality factor comparison of 17 and 18-period micro-gears. (d) Spatial distribution of strain before (solid blue line) and after (dashed blue line) excitation (2 mW) overlaid on the electric field profile of  $\text{TE}_{(19,1)}$  in an 18-period micro-gear. (e) Spatial distribution of strain before (solid blue line) and after (dashed blue line) excitation (2 mW) overlaid on the electric field profile of  $\text{TE}_{(11,3)}$  in a 17-period micro-gear.

However, the heat-induced power-dependent Raman shift must be eliminated. Given that the total Raman shift can be expressed as in Eq. (1),

$$\Delta\omega = \underbrace{\gamma_T\Delta T + \gamma_\varepsilon\alpha_{TEC}\Delta T}_{\text{Excitation}} + \underbrace{\gamma_\varepsilon\varepsilon}_{\text{Stressor-layer}}, \quad (1)$$

$$\Delta\omega(p) = \underbrace{\Delta\omega_T(p) + \Delta\omega_\alpha(p)}_{\text{Dynamic}} + \underbrace{\Delta\omega_\varepsilon}_{\text{Static}}, \quad (2)$$

where  $\Delta\omega$  is the total Raman shift in wavenumbers ( $\text{cm}^{-1}$ ). It is determined by two main factors that can be categorized as dynamic—due to excitation—thus dependent on the power used and the corresponding heat generated, and static—due to the forces applied by the stressor layer independent of the excitation, as expressed in Eq. (2). The excitation effect on the Raman shift is resembled in the first two terms; the first dynamic term ( $\gamma_T\Delta T$ ) accounts for pure heating effects, where  $\gamma_T$  is the sensitivity of the Raman shift to the change in temperature  $\Delta T$  in a stress-free condition, or a pure phonon–phonon interaction.<sup>59,60</sup> This term always adds up to the Raman redshift. In addition, the second dynamic term ( $\gamma_\varepsilon\alpha_{TEC}\Delta T$ ) indicates the shift due to the change in the lattice constant due to the thermal expansion imposed by  $\Delta T$  upon excitation. This effect is governed by the thermal expansion coefficient ( $\alpha_{TEC}$ ) and the Raman shift sensitivity toward the strain  $\gamma_\varepsilon$ . If the excited layer is not constrained by fixed boundaries, the thermal expansion will always contribute a redshift to the Raman peak due to the increase in the lattice constant due to heating. This is not the case in our devices since the thermal expansion coefficient of the Ge cavity is higher than that of the encapsulating  $\text{SiO}_2$  stressor layer, restricting its expansion. These two terms are power dependent, as the temperature of the device is directly related to the excitation power. It should be noted that the total Raman sensitivity to heating,  $\gamma_p$ , can be combined as  $\gamma_p = \gamma_T + \gamma_\varepsilon\alpha_{TEC}$ , bearing in mind that Eq. (1) is assumed to be unidirectional in space for simplicity.<sup>60</sup> The sensitivity of the Raman shift to temperature in stress-free Ge layers is reported to be  $-0.016 \text{ cm}^{-1} \text{ K}^{-1}$ .<sup>61</sup> As the sensitivity to temperature can be correlated with the absorbed power, this sensitivity to excitation is reported as equivalent to  $-0.094 \text{ cm}^{-1} \text{ mW}^{-1}$ .<sup>61</sup> Note that this value corresponds to the net effect of the two dynamic terms in Eq. (2). The third term is power-independent as it reflects the change in the lattice constant, or the strain ( $\varepsilon$ ), due to the mechanical forces applied by the stressor layer in our case. This shift is also proportional to the strain sensitivity factor  $\gamma_\varepsilon$ . The values of this proportionality factor are reported to be  $152$  ( $390$ )  $\text{cm}^{-1}$  for the uniaxial (biaxial) strain of Ge.<sup>40,41,62,63</sup> If the forces applied by the stressor layer are tensile in nature, a redshift is expected due to this term.

Registering the Raman peak positions vs the excitation power values in Fig. 4(b), the Raman shift relative to bulk Ge at  $302 \text{ cm}^{-1}$  as a function of power ( $\Delta\omega(p)$ ) can be fitted using a linear function as  $\Delta\omega(p) = -1.509 \times p - 1$ , where  $p$  is in milliwatts. The excitation-free strain value is proportional to the power-independent term according to Eq. (1), which can also be expressed as  $\lim_{p \rightarrow 0^+} \Delta\omega(p)$ , resulting in  $-1 \text{ cm}^{-1}$  (the strained Ge peak at  $301 \text{ cm}^{-1}$ ), the y-intercept of the linear-fit equation. The strain value can then be estimated by dividing the Raman shift over the proportionality

factor  $\gamma_\varepsilon$ ; accordingly, an accurate estimation of the 0.26% biaxial tensile strain value can be obtained in this particular device. Remarkable to our discussion, the sensitivity of the Raman shift to excitation  $\gamma_p$  is  $-1.509 \text{ cm}^{-1} \text{ mW}^{-1}$ . Note that the magnitude of this sensitivity is over 16 times higher than that of stress-free Ge layers ( $-0.094 \text{ cm}^{-1} \text{ mW}^{-1}$ ),<sup>61</sup> indicating either a higher increase in temperature per unit of excitation, or a larger thermal expansion due to the same increase in temperature. The latter explanation is unlikely as our platform has constraining boundaries compared to the reference Ge film. The former explanation is more convincing as a Ge cavity encapsulated with films of poor thermal conductivity is expected to undergo a higher increase in temperature compared to a continuous Ge film due to the reduced heat sinking area. Yet, this sensitivity term can also be mapped to the average cavity temperatures estimated by simulations; considering an average temperature of  $\sim 275^\circ\text{C}$  at 2.2 mW excitation and a temperature of  $25^\circ\text{C}$  of the non-excited cavity, the Raman-shift sensitivity to temperature can be calculated as  $-0.0132 \text{ cm}^{-1} \text{ K}^{-1}$ . Remarkably, this is lower in magnitude than the value reported for stress-free Ge of  $-0.016 \text{ cm}^{-1} \text{ K}^{-1}$ .<sup>61</sup> This indicates that a lower Raman shift is expected in our devices compared to Ge films at the same temperature. Bearing in mind that this sensitivity comprises pure heating effects and thermal-expansion effects, the thermal expansion component can explain measuring a lower Raman shift at a certain temperature. For instance, if we consider the 18-period micro-gear with an average temperature of  $275^\circ\text{C}$  (2.2 mW), the Raman peak is expected to be measured at  $\sim 297 \text{ cm}^{-1}$  ( $\Delta\omega = 4 \text{ cm}^{-1}$ ) in a stress-free Ge layer with no constraining  $\text{SiO}_2$  encapsulation. In our case, the peak is at  $297.7 \text{ cm}^{-1}$  ( $\Delta\omega = 3.3 \text{ cm}^{-1}$ ), or slightly blueshifted by a factor of  $0.7 \text{ cm}^{-1}$ . This effect is due to the complex boundary constraints limiting the thermal expansion, imposing relative compression forces on the Ge cavity, or a blueshift of the Raman peak. This result coincides with the strain simulations upon excitation in Fig. 3(b). Similar effects are observed in the literature in the form of mechanical buckling, resulting in wrinkles or ripples in the expanding films undergoing thermal excitation with fixed boundaries or constraints of lower thermal expansion coefficients.<sup>59</sup>

#### D. Strain and mode overlap

To visualize this effect and its implications on WGMs with different orders, simulated strain values before (0 mW) and after (2 mW) excitation of even (18) and odd (17) parity micro-gears are plotted in Figs. 4(d) and 4(e). A first-radial-order WGM is considered an exemplar WGM in the 18-period cavity in Fig. 4(d). For comparison, a third-radial-order WGM is considered as an example in the 17-period cavity in Fig. 4(e). The electric field profiles of  $\text{TE}_{(19,1)}$  and  $\text{TE}_{(11,3)}$  are plotted across the diameter of the cavities, as shown in Figs. 4(d) and 4(e), respectively, overlaid on the strain profiles before (solid) and after (dashed) excitation. Note that the number of electric field maxima along the radius of the cavity is the radial order of the WGM. Higher-order WGM  $\text{TE}_{(11,3)}$  has its field maxima nearer to the center of the cavity compared to the first-order WGM  $\text{TE}_{(19,1)}$ , with the mode's peak at the inner circumference. Initially, both cavities experience similar volumetric tensile strain, with a maximum value of around 0.8%, according to simulations. This tensile strain value is estimated across the diameter of



the cavity in the middle of the Ge layer. Higher tensile strain values are expected at the bottom of the Ge layer due to the upward deformation before excitation, as shown in Fig. 3(a), and lower values are expected on top for the same reason.<sup>12</sup> It is evident that the strain has lower values in the middle and at the circumference of the cavity, while being fairly uniform in between. The WGMs have negligible overlap with the middle of the cavity, yet the first-radial-order WGMs are more sensitive to the strain values at the circumference,<sup>18</sup> as a larger portion of the electric field dwells in that region compared to higher-radial-order modes. For this reason, in addition to experiencing more scattering losses due to the vicinity to the rough etched surfaces, first-radial-order WGMs may have lower quality factors at lower excitation power values. This hypothesis agrees with the quality factors measured for TE<sub>(11,3)</sub> and TE<sub>(19,1)</sub> as shown in Fig. 4(c), where the higher-radial-order WGM TE<sub>(11,3)</sub> initially has a significantly better quality factor. As the excitation power increases, the strain profile undergoes a reduction in value and becomes more uniform [dashed line, Figs. 4(d) and 4(e)] as the cavity deforms downward [Fig. 3(b)]. Remarkably, the quality factor of TE<sub>(11,3)</sub> drops faster than TE<sub>(19,1)</sub>; the drop itself for both modes can be expected as the heat-induced strain profile is degraded, decreasing the strain-originated optical gain. The faster degradation behavior of TE<sub>(11,3)</sub> is probably more influenced by the vicinity of its electric field to the excitation region in the middle, where higher temperatures are expected, compared to the circumference. It is worth mentioning in this context that heat dissipation by radiation through the cavity's surface is neglected in our study. If it is to be considered, then the temperature is expected to be even less than the current estimation at the circumference compared to the central regions, adding to the favor of first-radial-order WGMs and even-parity micro-gears in this aspect. This indicates that a well-performing laser source relying on a stressor layer as a source of optical gain must mitigate heating effects through heat-sinking techniques, match the thermal expansion coefficients of the cavity and the stressor layer, and target an optical mode with a good overlap with the tensile strain and temperature profiles upon excitation.

## V. CONCLUSION

Ge-based micro-cavities with all-around stressor layers are popular platforms for Ge and GeSn-based laser sources. Recent studies have focused on enhancing tensile strain and mitigating heating effects for efficient RT operation. The heating effects are often considered from the traditional optical and carrier loss mechanisms point of view. In this work, we have investigated the effect of excitation on the strain profile within such platforms, emphasizing its importance for the optical gain in indirect-gap materials. Ge micro-cavities with all-around stressor layers were fabricated and characterized using Raman spectroscopy and PL measurements. The behavior of PL and Raman spectra vs different excitation powers was analyzed to understand the dynamic effect of heating on the strain. Experimental redshift values in both types of spectra were found to be less than the theoretical estimations for stress-free Ge layers, indicating a source of mechanical compression or reduction in tensile strain upon excitation. FEM simulations were performed to visualize this transient behavior, confirming the outcomes of the theoretical analysis. It was found that the difference in thermal expansion

coefficients between the cavity and the stressor layer creates a complex boundary condition for the cavity, restricting its expansion with excitation in the studied power range. This effect deforms the cavity, altering its strain profile and directly affecting the optical gain values in Ge-based cavities. We believe that this study outlines an important type of mechanically originated optical loss mechanism, crucial for group-IV laser sources relying on strain as a main source of optical gain.

## ACKNOWLEDGMENTS

We would like to acknowledge our research collaborators, engineers, and line managers at Al Hussein Technical University and the University of Southampton for supporting this project.

## AUTHOR DECLARATIONS

### Conflict of Interest

The authors have no conflicts to disclose.

## Author Contributions

**Abdelrahman Z. Al-Attili:** Conceptualization (lead); Data curation (lead); Formal analysis (lead); Investigation (lead); Methodology (equal); Writing – original draft (lead). **Daniel Burt:** Investigation (supporting); Writing – review & editing (supporting). **Tasmiat Rahman:** Software (supporting); Validation (supporting). **Zuo Li:** Investigation (supporting). **Naoki Higashitarumizu:** Investigation (supporting). **Frederic Y. Gardes:** Software (supporting); Supervision (supporting). **Yasuhiko Ishikawa:** Investigation (supporting); Methodology (supporting); Resources (supporting). **Shinichi Saito:** Supervision (supporting); Writing – review & editing (supporting).

## DATA AVAILABILITY

The data that support the findings of this study are available from the corresponding author upon reasonable request.

## REFERENCES

- S. Saito, F. Y. Gardes, A. Z. Al-Attili, K. Tani, K. Oda, Y. Suwa, T. Ido, Y. Ishikawa, S. Kako, S. Iwamoto, and Y. Arakawa, "Group IV light sources to enable the convergence of photonics and electronics," *Front. Mater.* **1**, 15 (2014).
- S. Saito, A. Z. Al-Attili, K. Oda, and Y. Ishikawa, "Towards monolithic integration of germanium light sources on silicon chips," *Semicond. Sci. Technol.* **31**, 043002 (2016).
- B. Wang, E. Sakat, E. Herth, M. Gromovyi, A. Bjelajac, J. Chaste, G. Patriarche, P. Boucaud, F. Boeuf, N. Pauc, V. Calvo, J. Chrétien, M. Frauenrath, A. Chelnokov, V. Reboud, J. M. Hartmann, and M. El Kurdi, "GeSnOI mid-infrared laser technology," *Light: Sci. Appl.* **10**, 232 (2021).
- J. Liu, R. Camacho-Aguilera, J. T. Bessette, X. Sun, X. Wang, Y. Cai, L. C. Kimerling, and J. Michel, "Ge-on-Si optoelectronics," *Thin Solid Films* **520**, 3354–3360 (2012).
- J. Liu, L. C. Kimerling, and J. Michel, "Monolithic Ge-on-Si lasers for large-scale electronic–photonic integration," *Semicond. Sci. Technol.* **27**, 094006 (2012).
- J. Liu, X. Sun, R. Camacho-Aguilera, L. C. Kimerling, and J. Michel, "Ge-on-Si laser operating at room temperature," *Opt. Lett.* **35**, 679–681 (2010).

- <sup>7</sup>R. E. Camacho-Aguilera, Y. Cai, N. Patel, J. T. Bessette, M. Romagnoli, L. C. Kimerling, and J. Michel, "An electrically pumped germanium laser," *Opt. Express* **20**, 11316–11320 (2012).
- <sup>8</sup>R. E. Camacho-Aguilera, Y. Cai, J. Bessette, L. C. Kimerling, and J. Michel, "High active carrier concentration in n-type, thin film Ge using delta-doping," *Opt. Mater. Express* **2**, 1462–1469 (2012).
- <sup>9</sup>R. Camacho-Aguilera, Z. Han, Y. Cai, L. C. Kimerling, and J. Michel, "Direct band gap narrowing in highly doped Ge," *Appl. Phys. Lett.* **102**, 152106 (2013).
- <sup>10</sup>A. Z. Al-Attili, S. Kako, M. Husain, F. Gardes, N. Higashitarumizu, S. Iwamoto, Y. Arakawa, Y. Ishikawa, H. Arimoto, K. Oda, T. Ido, and S. Saito, "Whispering gallery mode resonances from Ge micro-disks on suspended beams," *Front. Mater.* **2**, 43 (2015).
- <sup>11</sup>A. Al-Attili, M. Husain, F. Gardes, H. Arimoto, S. Saito, N. Higashitarumizu, Y. Ishikawa, S. Kako, S. Iwamoto, and Y. Arakawa, "Fabrication of Ge micro-disks on free-standing SiO<sub>2</sub> beams for monolithic light emission," in *Proc. 15th IEEE Conf. Nanotechnology (IEEE NANO) (IEEE, 2015)*, pp. 1274–1277.
- <sup>12</sup>A. Z. Al-Attili, S. Kako, M. K. Husain, F. Y. Gardes, S. Iwamoto, Y. Arakawa, and S. Saito, "Tensile strain engineering of germanium micro-disks on free-standing SiO<sub>2</sub> beams," *Jpn. J. Appl. Phys.* **55**, 04EH02 (2016).
- <sup>13</sup>A. Z. Al-Attili, D. Burt, Z. Li, N. Higashitarumizu, F. Y. Gardes, K. Oda, Y. Ishikawa, and S. Saito, "Germanium vertically light-emitting micro-gears generating orbital angular momentum," *Opt. Express* **26**, 34675–34688 (2018).
- <sup>14</sup>A. Z. Al-Attili, D. Burt, Z. Li, N. Higashitarumizu, F. Gardes, Y. Ishikawa, and S. Saito, "Chiral germanium micro-gears for tuning orbital angular momentum," *Sci. Rep.* **12**, 7465 (2022).
- <sup>15</sup>A. Ghrib, M. de Kersauson, M. El Kurdi, R. Jakomin, G. Beaudoin, S. Sauvage, G. Fishman, G. Ndong, M. Chaigneau, R. Ossikovski, I. Sagnes, and P. Boucaud, "Control of tensile strain in germanium waveguides through silicon nitride layers," *Appl. Phys. Lett.* **100**, 201104 (2012).
- <sup>16</sup>A. Ghrib, M. El Kurdi, M. de Kersauson, M. Prost, S. Sauvage, X. Checoury, G. Beaudoin, I. Sagnes, and P. Boucaud, "Tensile-strained germanium microdisks," *Appl. Phys. Lett.* **102**, 221112 (2013).
- <sup>17</sup>A. Ghrib, M. El Kurdi, M. Prost, M. de Kersauson, L. Largeau, O. Mauguin, G. Beaudoin, S. Sauvage, X. Checoury, G. Ndong, M. Chaigneau, R. Ossikovski, S. David, I. Sagnes, and P. Boucaud, "Strain engineering in germanium microdisks," *Proc. SPIE* **8990**, 89901C (2014).
- <sup>18</sup>A. Ghrib, M. El Kurdi, M. Prost, S. Sauvage, X. Checoury, G. Beaudoin, M. Chaigneau, R. Ossikovski, I. Sagnes, and P. Boucaud, "All-around SiN stressor for high and homogeneous tensile strain in germanium microdisk cavities," *Adv. Opt. Mater.* **3**, 353–358 (2015).
- <sup>19</sup>D. Nam, D. Sukhdeo, A. Roy, K. Balram, S. L. Cheng, K. C. Y. Huang, Z. Yuan, M. Brongersma, Y. Nishi, D. Miller, and K. Saraswat, "Strained germanium thin film membrane on silicon substrate for optoelectronics," *Opt. Express* **19**, 25866–25872 (2011).
- <sup>20</sup>D. Nam, D. Sukhdeo, S.-L. Cheng, A. Roy, K. Chih-Yao Huang, M. Brongersma, Y. Nishi, and K. Saraswat, "Electroluminescence from strained germanium membranes and implications for an efficient Si-compatible laser," *Appl. Phys. Lett.* **100**, 131112 (2012).
- <sup>21</sup>D. Nam, D. S. Sukhdeo, J. H. Kang, J. Petykiewicz, J. H. Lee, W. S. Jung, J. Vučković, M. L. Brongersma, and K. C. Saraswat, "Strain-induced pseudoheterostructure nanowires confining carriers at room temperature with nanoscale-tunable band profiles," *Nano Lett.* **13**, 3118–3123 (2013).
- <sup>22</sup>D. Nam, J. H. Kang, M. L. Brongersma, and K. C. Saraswat, "Observation of improved minority carrier lifetimes in high-quality Ge-on-insulator using time-resolved photoluminescence," *Opt. Lett.* **39**, 6205–6208 (2014).
- <sup>23</sup>D. Nam, D. S. Sukhdeo, S. Gupta, J. H. Kang, M. L. Brongersma, and K. C. Saraswat, "Study of carrier statistics in uniaxially strained Ge for a low-threshold Ge laser," *IEEE J. Sel. Top. Quantum Electron.* **20**, 1500107 (2014).
- <sup>24</sup>A. Elbaz, D. Buca, N. von den Driesch, K. Pantzas, G. Patriarche, N. Zerounian, E. Herth, X. Checoury, S. Sauvage, I. Sagnes, A. Foti, R. Ossikovski, J. M. Hartmann, F. Boeuf, Z. Ikonik, P. Boucaud, D. Grützmacher, and M. El Kurdi, "Ultra-low-threshold continuous-wave and pulsed lasing in tensile-strained GeSn alloys," *Nat. Photonics* **14**, 375–382 (2020).
- <sup>25</sup>D. Buca, A. Bjelajac, D. Spirito, O. Concepción, M. Gromovyi, E. Sakat, X. Lafosse, L. Ferlazzo, N. von den Driesch, Z. Ikonik, D. Grützmacher, G. Capellini, and M. El Kurdi, "Room temperature lasing in GeSn microdisks enabled by strain engineering," *Adv. Opt. Mater.* **10**, 2201024 (2022).
- <sup>26</sup>A. Bjelajac, M. Gromovyi, E. Sakat, B. Wang, G. Patriarche, N. Pauc, V. Calvo, P. Boucaud, F. Boeuf, A. Chelnokov, V. Reboud, M. Frauenrath, J. M. Hartmann, and M. El Kurdi, "Up to 300 K lasing with GeSn-On-insulator microdisk resonators," *Opt. Express* **30**, 3954–3961 (2022).
- <sup>27</sup>J. Chrétien, Q. M. Thai, M. Frauenrath, L. Casiez, A. Chelnokov, V. Reboud, J. M. Hartmann, M. El Kurdi, N. Pauc, and V. Calvo, "Room temperature optically pumped GeSn microdisk lasers," *Appl. Phys. Lett.* **120**, 051107 (2022).
- <sup>28</sup>M. El Kurdi, G. Fishman, S. Sauvage, and P. Boucaud, "Band structure and optical gain of tensile-strained germanium based on a 30 band k-p formalism," *J. Appl. Phys.* **107**, 013710 (2010).
- <sup>29</sup>H. Tahini, A. Chronos, R. Grimes, U. Schwingenschlögl, and A. Dimoulas, "Strain-induced changes to the electronic structure of germanium," *J. Phys.: Condens. Matter* **24**, 195802 (2012).
- <sup>30</sup>A. Z. Al-Attili, S. Kako, M. K. Husain, F. Y. Gardes, H. Arimoto, N. Higashitarumizu, S. Iwamoto, Y. Arakawa, Y. Ishikawa, and S. Saito, "Spin-on doping of germanium-on-insulator wafers for monolithic light sources on silicon," *Jpn. J. Appl. Phys.* **54**, 052101 (2015).
- <sup>31</sup>B. Dutt, D. S. Sukhdeo, D. Nam, B. M. Vulovic, Z. Yuan, and K. C. Saraswat, "Roadmap to an efficient germanium-on-silicon laser: Strain vs. n-type doping," *IEEE Photonics J.* **4**, 2002–2009 (2012).
- <sup>32</sup>J. Liu, X. Sun, D. Pan, X. Wang, L. C. Kimerling, T. L. Koch, and J. Michel, "Tensile-strained, n-type Ge as a gain medium for monolithic laser integration on Si," *Opt. Express* **15**, 11272–11277 (2007).
- <sup>33</sup>J. Liu, X. Sun, L. C. Kimerling, and J. Michel, "Direct-gap optical gain of Ge on Si at room temperature," *Opt. Lett.* **34**, 1738–1740 (2009).
- <sup>34</sup>D. Cammilleri, F. Fossard, D. Débarre, C. Tran Manh, C. Dubois, E. Bustarret, C. Marcenat, P. Achatz, D. Bouchier, and J. Boulmer, "Highly doped Si and Ge formed by GILD (gas immersion laser doping); from GILD to superconducting silicon," *Thin Solid Films* **517**, 75–79 (2008).
- <sup>35</sup>H. A. Tahini, A. Chronos, R. W. Grimes, and U. Schwingenschlögl, "Co-doping with antimony to control phosphorous diffusion in germanium," *J. Appl. Phys.* **113**, 073704 (2013).
- <sup>36</sup>L. Carroll, P. Friedli, S. Neuenschwander, H. Sigg, S. Cecchi, F. Isa, D. Christina, G. Isella, Y. Fedoryshyn, and J. Faist, "Direct-gap gain and optical absorption in germanium correlated to the density of photoexcited carriers, doping, and strain," *Phys. Rev. Lett.* **109**, 057402 (2012).
- <sup>37</sup>F. T. A. Pilon, A. Lyaota, Y.-M. Niquet, V. Reboud, V. Calvo, N. Pauc, J. Widiez, C. Bonzon, J. M. Hartmann, A. Chelnokov, J. Faist, and H. Sigg, "Lasing in strained germanium microbridges," *Nat. Commun.* **10**, 2724 (2019).
- <sup>38</sup>S. Bao, D. Kim, C. Onwukaeme, S. Gupta, K. Saraswat, K. H. Lee, Y. Kim, D. Min, Y. Jung, H. Qiu, H. Wang, E. A. Fitzgerald, C. S. Tan, and D. Nam, "Low-threshold optically pumped lasing in highly strained germanium nanowires," *Nat. Commun.* **8**, 1845 (2017).
- <sup>39</sup>J. R. Jain, D. S. Ly-Gagnon, K. C. Balram, J. S. White, M. L. Brongersma, D. A. B. Miller, and R. T. Howe, "Tensile-strained germanium-on-insulator substrate fabrication for silicon-compatible optoelectronics," *Opt. Mater. Express* **1**, 1121–1126 (2011).
- <sup>40</sup>M. J. Süess, R. Geiger, R. A. Minamisawa, G. Schiefler, J. Frigerio, D. Christina, G. Isella, R. Spolenak, J. Faist, and H. Sigg, "Analysis of enhanced light emission from highly strained germanium microbridges," *Nat. Photonics* **7**, 466–472 (2013).
- <sup>41</sup>D. S. Sukhdeo, D. Nam, J. H. Kang, M. L. Brongersma, and K. C. Saraswat, "Direct bandgap germanium-on-silicon inferred from 57% (100) uniaxial tensile strain [Invited]," *Photonics Res.* **2**, A8–A13 (2014).
- <sup>42</sup>M. El Kurdi, M. Prost, A. Ghrib, S. Sauvage, X. Checoury, G. Beaudoin, I. Sagnes, G. Picardi, R. Ossikovski, and P. Boucaud, "Direct band gap germanium microdisks obtained with silicon nitride stressor layers," *ACS Photonics* **3**, 443–448 (2016).
- <sup>43</sup>M. Virgilio, C. L. Manganelli, G. Grosso, T. Schroeder, and G. Capellini, "Photoluminescence, recombination rate, and gain spectra in optically excited n-type and tensile strained germanium layers," *J. Appl. Phys.* **114**, 243102 (2013).

- <sup>44</sup>D. Burt, A. Al-Attili, Z. Li, F. Gardès, M. Sotto, N. Higashitarumizu, Y. Ishikawa, K. Oda, O. M. Querin, S. Saito, and R. Kelsall, "Enhanced light emission from improved homogeneity in biaxially suspended germanium membranes from curvature optimization," *Opt. Express* **25**, 22911–22922 (2017).
- <sup>45</sup>R. W. Millar, K. Gallacher, J. Frigerio, A. Ballabio, A. Bashir, I. MacLaren, G. Isella, and D. J. Paul, "Analysis of Ge micro-cavities with in-plane tensile strains above 2%," *Opt. Express* **24**, 4365–4374 (2016).
- <sup>46</sup>D. Burt, J. Gonzales, A. Z. Al-Attili, H. Rutt, A. Z. Khokar, K. Oda, F. Gardes, and S. Saito, "Comparison of uniaxial and polyaxial suspended germanium bridges in terms of mechanical stress and thermal management towards a CMOS compatible light source," *Opt. Express* **27**, 37846–37858 (2019).
- <sup>47</sup>K. Tani, K. Oda, M. Deura, and T. Ido, "Enhanced room-temperature electroluminescence from a germanium waveguide on a silicon-on-insulator diode with a silicon nitride stressor," *Opt. Express* **29**, 3584–3595 (2021).
- <sup>48</sup>M. Fujita and T. Baba, "Microgear laser," *Appl. Phys. Lett.* **80**, 2051–2053 (2002).
- <sup>49</sup>K. Nozaki, A. Nakagawa, D. Sano, and T. Baba, "Ultralow threshold and single-mode lasing in microgear lasers and its fusion with quasi-periodic photonic crystals," *IEEE J. Sel. Top. Quantum Electron.* **9**, 1355–1360 (2003).
- <sup>50</sup>Y. Ishikawa, K. Wada, D. D. Cannon, J. Liu, H. C. Luan, and L. C. Kimerling, "Strain-induced band gap shrinkage in Ge grown on Si substrate," *Appl. Phys. Lett.* **82**, 2044–2046 (2003).
- <sup>51</sup>G. G. Stoney, "The tension of metallic films deposited by electrolysis," *Proc. R. Soc. London, Ser. A* **82**, 172–175 (1909).
- <sup>52</sup>V. K. Yang, M. Groenert, C. W. Leitz, A. J. Pitera, M. T. Currie, and E. A. Fitzgerald, "Crack formation in GaAs heteroepitaxial films on Si and SiGe virtual substrates," *J. Appl. Phys.* **93**, 3859–3865 (2003).
- <sup>53</sup>G. K. White, "Thermal expansion of reference materials: Copper, silica and silicon," *J. Phys. D: Appl. Phys.* **6**, 2070 (1973).
- <sup>54</sup>G. Carlotti, L. Doucet, and M. Dupeux, "Comparative study of the elastic properties of silicate glass films grown by plasma enhanced chemical vapor deposition," *J. Vac. Sci. Technol. B* **14**, 3460–3464 (1996).
- <sup>55</sup>G. Carlotti, L. Doucet, and M. Dupeux, "Elastic properties of silicon dioxide films deposited by chemical vapour deposition from tetraethylorthosilicate," *Thin Solid Films* **296**, 102–105 (1997).
- <sup>56</sup>X. Sun, J. Liu, L. C. Kimerling, and J. Michel, "Direct gap photoluminescence of *n*-type tensile-strained Ge-on-Si," *Appl. Phys. Lett.* **95**, 011911 (2009).
- <sup>57</sup>H. H. Li, "Refractive index of silicon and germanium and its wavelength and temperature derivatives," *J. Phys. Chem. Ref. Data* **9**, 561–658 (1980).
- <sup>58</sup>H. W. Icenogle, B. C. Platt, and W. L. Wolfe, "Refractive indexes and temperature coefficients of germanium and silicon," *Appl. Opt.* **15**, 2348–2351 (1976).
- <sup>59</sup>X. Huang, Y. Gao, T. Yang, W. Ren, H. M. Cheng, and T. Lai, "Quantitative analysis of temperature dependence of Raman shift of monolayer WS<sub>2</sub>," *Sci. Rep.* **6**, 32236 (2016).
- <sup>60</sup>S. Huang, Y. Chen, Z. Luo, and X. Xu, "Temperature and strain effects in micro-Raman thermometry for measuring in-plane thermal conductivity of thin films," *Nanoscale Microscale Thermophys. Eng.* **25**, 91–100 (2021).
- <sup>61</sup>J. Jaramillo-Fernandez, E. Chavez-Angel, and C. M. Sotomayor-Torres, "Raman thermometry analysis: Modelling assumptions revisited," *Appl. Therm. Eng.* **130**, 1175–1181 (2018).
- <sup>62</sup>G. Capellini, G. Kozłowski, Y. Yamamoto, M. Lisker, C. Wenger, G. Niu, P. Zaumseil, B. Tillack, A. Ghrib, M. de Kersauson, M. El Kurdi, P. Boucaud, and T. Schroeder, "Strain analysis in SiN/Ge microstructures obtained via Si-complementary metal oxide semiconductor compatible approach," *J. Appl. Phys.* **113**, 013513 (2013).
- <sup>63</sup>G. Capellini, C. Reich, S. Guha, Y. Yamamoto, M. Lisker, M. Virgilio, A. Ghrib, M. El Kurdi, P. Boucaud, B. Tillack, and T. Schroeder, "Tensile Ge microstructures for lasing fabricated by means of a silicon complementary metal-oxide-semiconductor process," *Opt. Express* **22**, 399–410 (2014).